Determination of phonon dispersion curves by means of inelastic x-ray scattering

2001 J. Phys.: Condens. Matter 13 7627

(http://iopscience.iop.org/0953-8984/13/34/310)

INSTITUTE OF PHYSICS PUBLISHING JOURNAL OF PHYSICS: CONDENSED MATTER

J. Phys.: Condens. Matter **13** (2001) 7627–7644 PII: S0953-8984(01)24544-5

Determination of phonon dispersion curves by means of inelastic x-ray scattering

Eberhard Burkel

Physics of New Materials, Department of Physics, University of Rostock, August-Bebel-Strasse 55, 18055 Rostock, Germany

E-mail: eberhard.burkel@physik.uni-rostock.de

Received 3 May 2001
Published 9 August 2001
Online at stacks.iop.org/JPhysCM/13/7627

Abstract

The inelastic x-ray scattering technique using the brilliant x-ray beams from synchrotron radiation sources is perfectly well suited for the determination of the dispersion curves of phonon modes in condensed matter. In this contribution some experimental details of the method are discussed. The strengths are demonstrated with several recent results.

(Some figures in this article are in colour only in the electronic version)

1. Introduction

In the early days of x-ray scattering in condensed matter physics the diffraction spots delivered information on the static order of the atoms in the material investigated. Attempts were soon made to analyse the diffuse scattering intensities visible between the diffraction spots. It was expected that the thermal movements of the atoms would contribute to these intensities which, for this reason, contain information on the lattice dynamics.

One of the first experiments was performed by Walker (1956), with measurements of the diffuse scattering intensity along high-symmetry directions from fcc aluminium (figure 1(a)) in reciprocal space. From these data the phonon dispersion curves shown in figure 1(b) were derived using a model of elastic waves describing the motions of the atoms, according to the lattice dynamics theory of Born (1942).

Recently, the thermal diffuse scattering intensity of a thin Si wafer (0.5 mm) was recorded in transmission Laue geometry using the high photon flux of an undulator beam at the Advanced Photon Source (APS) in Chicago by Holt *et al* (1999). Figure 2 shows the intensity distributions detected by an image plate for Si(111) in (a) and for Si(100) in (b). Figures 2(c) and 2(d) are best fits to the x-ray intensity pattern obtained by model calculations of the lattice dynamics, in agreement with neutron data from the literature.

However, nowadays it is possible to measure dispersion curves directly by the detection of energy shifts of the photons occurring in the inelastic scattering process due to the creation and

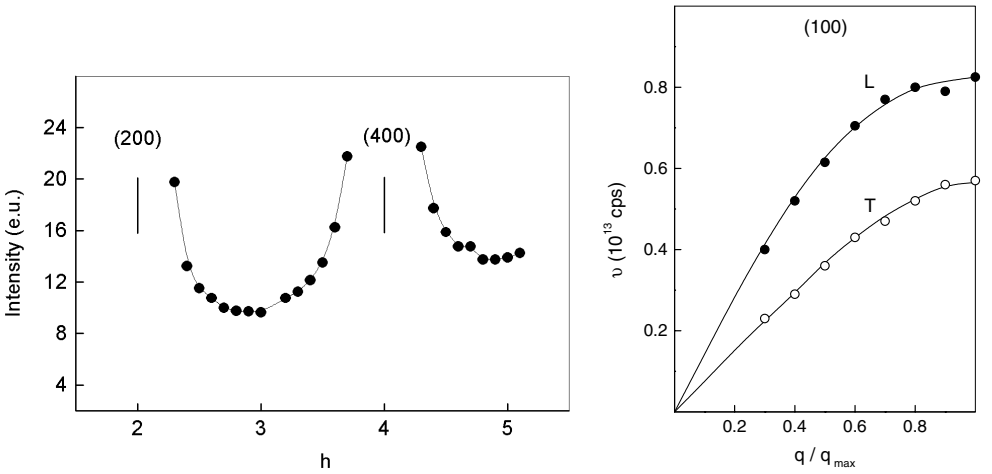

Figure 1. (a) Diffuse x-ray scattering intensities for fcc Al along the [h00] direction and (b) the derived phonon dispersion curves for fcc Al, after Walker (1956).

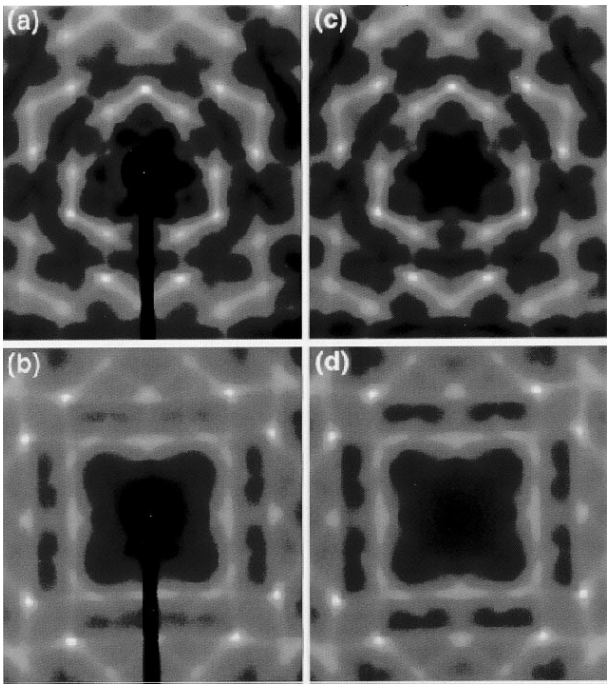

Figure 2. Transmission x-ray scattering images taken from (a) Si(111) and (b) Si(100). In each case the shadow of a beam stop is visible. (c) and (d) show calculated images for these orientations (Holt *et al* 1999).

annihilation of vibrational quanta (Burkel *et al* 1986, 1987a, b, 1989, 1991, Dorner *et al* 1987, Burkel 1989, 1991, 2000). There is no need for model calculations to obtain the dispersion relations as is familiar from neutron scattering (Brockhouse 1961, Bacon 1962).

2. Scattering cross section

A general scattering experiment is shown schematically in figure 3. This arrangement is valid for all probes such as neutrons, electron beams and electromagnetic radiation. The incident beam of well defined wavevector $\boldsymbol{k}_i$, energy E_i and polarization unit vector $\boldsymbol{e}_i$ is scattered into the solid-angle element $d\Omega$ under the scattering angle 2θ. The scattered beam is completely defined by the new wavevector $\boldsymbol{k}_f$, the energy E_f and the polarization unit vector $\boldsymbol{e}_f$.

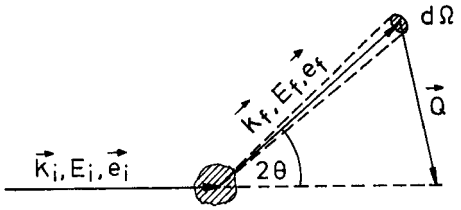

Figure 3. Scattering geometry.

The scattered intensity is described by the double-differential cross section $d^2\sigma/(d\Omega\, d\omega_f)$. It is given by the rate of removal of particles from the incident beam as the result of being scattered into a solid angle $d\Omega$ within a frequency range of $d\omega_f$.

The scattered beam is usually distributed over a range of energies E_f. There can be contributions of the beam that have been scattered elastically with no change of energy or other contributions that have changed energy due to inelastic scattering. Therefore, the scattering process contains information on energy and momentum transfers from

$$E = \hbar\omega \equiv E_i - E_f \qquad \hbar\boldsymbol{Q} \equiv \hbar(\boldsymbol{k}_i - \boldsymbol{k}_f). \tag{1}$$

The discussion will now concentrate on the scattering of x-rays where the transferred energy is normally smaller than the photon energy ($E \ll E_i$). In this case the momentum transfer $\hbar Q$ is simply connected with the scattering angle θ by

$$\hbar Q = 2\hbar k_i \sin\theta. \tag{2}$$

For further discussion of the double-differential scattering cross section the representation

$$\frac{d^2\sigma}{d\Omega\, d\omega_f} = \left(\frac{d\sigma}{d\Omega}\right)_0 S(\boldsymbol{Q}, \omega) \tag{3}$$

derived by Van Hove (1954), will be used. This description has the advantage of allowing separation of the double-differential cross section into two contributions. The coupling of the beam to the scattering system is characterized by the intrinsic cross section $(d\sigma/d\Omega)_0$, and the properties of the sample in the absence of the perturbing probe are expressed by the scattering function $S(\boldsymbol{Q}, \omega)$.

This treatment in the lowest-order Born approximation (first-order perturbation theory) is allowed, since the coupling of the electromagnetic field of the photon beam to the scattering electron system of the sample, given by the Thomson scattering cross section

$$\left(\frac{d\sigma}{d\Omega}\right)_0 = \left(\frac{d\sigma}{d\Omega}\right)_{Th} = r_0^2(\boldsymbol{e}_i \cdot \boldsymbol{e}_f)^2\left(\frac{\omega_f}{\omega_i}\right) \tag{4}$$

of a single electron, is weak. $r_0 = e^2/mc^2 = 2.818 \times 10^{-13}$ cm is the classical electron radius. Therefore, $(d\sigma/d\Omega)_{Th}$ is of the order of 10^{-25} cm^2. Since $E \ll E_i$, the factor ω_f/ω_i in (4) is about equal to 1 in the case of non-resonant x-ray scattering.

The scattering function can be discussed in different modifications. A sophisticated representation of the scattering function was derived by Van Hove (1954):

$$S(\boldsymbol{Q},\omega)=\frac{1}{2\pi}\int \mathrm{d}t\ \mathrm{e}^{-\mathrm{i}\omega t}\langle\Upsilon_\mathrm{i}|\sum_{j,j'}\mathrm{e}^{-\mathrm{i}\boldsymbol{Q}\cdot\boldsymbol{r}_j(t)}\mathrm{e}^{\mathrm{i}\boldsymbol{Q}\cdot\boldsymbol{r}_{j'}(0)}|\Upsilon_\mathrm{i}\rangle. \tag{5}$$

It describes the correlations of the scattering phases of the particles at positions $\boldsymbol{r}(0)$ with those at $\boldsymbol{r}_j(t)$ at different times t. In the classical limit it represents essentially the Fourier transform in time of the density correlation function and gives information on the particle fluctuations in the scattering system in the same states Υ_i at different times.

3. Phonon dispersion curves

3.1. Experimental determination

Inelastic scattering of x-rays from phonons is expected to supply similar information about the dynamics of the observed system to coherent inelastic neutron scattering. This is supported by the experiments of Joynson (1954) and Walker (1956), as discussed above. Within the limits of the adiabatic approximation, the electrons are expected to follow the movements of the nuclei instantaneously. This is reasonable since the vibrational motion of the atoms is orders of magnitude slower than typical electronic timescales. Therefore, phonons, i.e. low-frequency vibrations of the nuclei, will cause electron charge-density variations, which can be directly observed by inelastic x-ray scattering.

The scattering function (5) for one-phonon scattering can be written as

$$S(\boldsymbol{Q},\omega)=G(\boldsymbol{Q},\boldsymbol{q},j)F(\omega,T,\boldsymbol{q},j). \tag{6}$$

The dynamical structure factor $G(\boldsymbol{Q},\boldsymbol{q},j)$ is given by

$$G(\boldsymbol{Q},\boldsymbol{q},j)=\left|\sum_{d}^{\text{unit cell}} f_d(Q)\mathrm{e}^{-W_d}\left[\boldsymbol{Q}\cdot\boldsymbol{e}_d(\boldsymbol{q},j)\right]M_d^{-1/2}\mathrm{e}^{\mathrm{i}\boldsymbol{Q}\cdot\boldsymbol{d}}\right|^2. \tag{7}$$

$f_d(Q)$ is the atomic form factor of atom d at position $\boldsymbol{d}$ with $f_d(Q\to 0)=Z$. Z is the atomic number. $\boldsymbol{e}_d(\boldsymbol{q},j)$ is the component of the normalized phonon eigenvector in the mode j with phonon wavevector $\boldsymbol{q}$ for atom d. e^{-W_d} is the Debye–Waller factor of atom d and M_d is its mass. The function $F(\omega,T,\boldsymbol{q},j)$ for undamped phonons is given by

$$F(\omega,T,\boldsymbol{q},j)=\frac{\langle n\rangle+1/2\pm 1/2}{\omega_{q,j}}\delta(\omega\mp\omega_{q,j}). \tag{8}$$

Here the upper sign holds for energy loss and the lower one for energy gain by the x-rays. $\langle n\rangle$ is the Bose occupation factor and $\omega_{q,j}$ the frequency of phonon mode j with wavevector $\boldsymbol{q}$.

The scattering law for neutrons can be obtained from the scattering law for x-rays by simply replacing the atomic form factor by the Fermi scattering length.

Detailed discussions of the theory of phonons are given by Peierls (1955), Cochran and Cowley (1967), Horton and Maradudin (1974) and Brüsch (1982, 1986, 1987). The phonon eigenvectors $\boldsymbol{e}(\boldsymbol{q},j)$ describe the directions of the atomic vibrations in the unit cell of the crystal. In the main symmetry axes of crystals, two different types of vibrational mode exist (see figures 4(a), 4(b)), namely a longitudinal mode which is connected with atomic displacements parallel to the direction of the wavevector ($\boldsymbol{e}\parallel\boldsymbol{q}$), and a transverse wave which is connected with atomic displacements perpendicular to the direction of the wavevector ($\boldsymbol{e}\perp\boldsymbol{q}$). Therefore, the eigenvectors are also called polarization vectors. In general directions the vibrational modes are mixed.

$$\boldsymbol{Q}=\boldsymbol{k}_\mathrm{i}-\boldsymbol{k}_\mathrm{f}=\boldsymbol{\tau}+\boldsymbol{q} \tag{9}$$

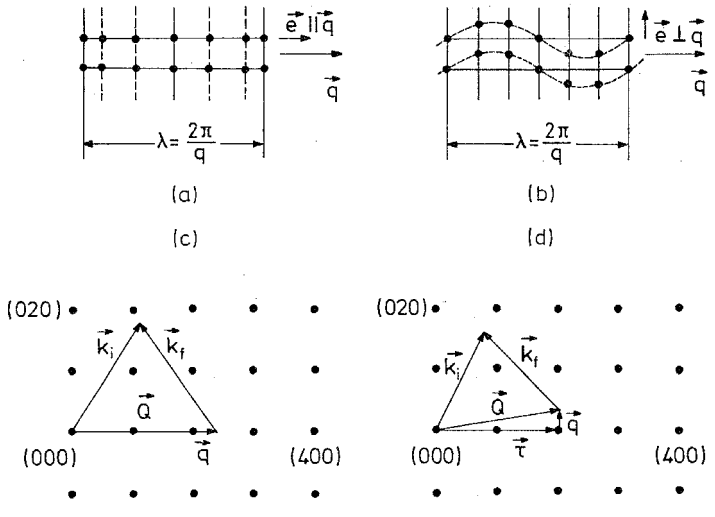

Figure 4. Atomic vibrations in the main symmetry direction of a crystal with longitudinal (a) and transverse (b) polarization in real space. Scattering geometry in reciprocal space for the measurement of a longitudinal (c) and transverse phonons (d) in the [100] direction.

where $\boldsymbol{q}$ is the phonon wavevector, defined with respect to the nearest reciprocal-lattice point $\boldsymbol{\tau}$. The directions of the polarization vector $\boldsymbol{e}(\boldsymbol{q})$ and the scattering vector $\boldsymbol{Q}$ select the type of vibrational mode to be detected, according to (7). An energy scan, called a constant-Q scan (see figure 5), with such a scattering vector will show two signals, due to the creation and the annihilation of a phonon.

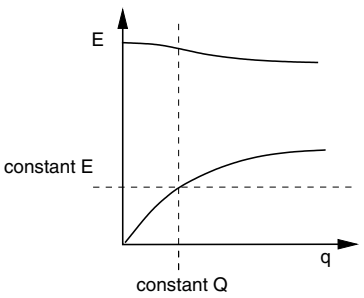

Figure 5. Phonon dispersion modes together with constant-Q and constant-E scan lines: schematic diagram.

The scattering geometry for detecting phonons in crystals is illustrated in figures 4(c), 4(d). It shows the positions of the scattering vectors in the reciprocal-space ($(hk0)$ plane) for the detection of longitudinal (figure 4(a)) and transverse (figure 4(b)) phonons in the [100] direction.

Certainly, the experimental scans for resolving phonon excitations can also be performed with constant energy and varying momentum transfers in constant-E scans (see figure 5).

The successful performance of a scattering experiment requires the knowledge of the resolution volume in energy and momentum space of a three-axis spectrometer. The detailed discussion of the resolution function by Dorner (1972) for the neutron case function also applies to x-rays.

Figure 6 shows the distribution of the wavevectors of the photons in an inelastic scattering process within the scattering plane of the reciprocal space. The sizes of the areas around the

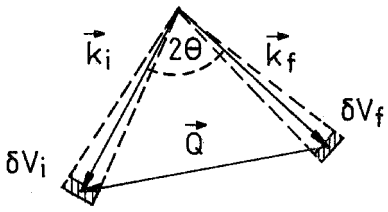

Figure 6. The distribution of photons in reciprocal space around the mean wavevectors $\boldsymbol{k}_\mathrm{i}$ and $\boldsymbol{k}_\mathrm{f}$.

mean wavevectors $\boldsymbol{k}_\mathrm{i}$ and $\boldsymbol{k}_\mathrm{f}$ depend essentially on the beam divergences, which are controlled by the sizes of the slits and by the illuminated areas on the monochromator and analyser. The folding of both contributions in all three dimensions leads, together with the energy resolution, to the complete resolution function $R(\boldsymbol{Q}, \omega)$.

It is known from neutron scattering (Cooper and Nathans 1967) that the resolution volume described by the function $R(\boldsymbol{Q}, \omega)$ has a certain inclination in the $(\boldsymbol{Q}, \omega)$ space. It is defined by the scattering angles of monochromator, sample and analyser of the three-axis spectrometer. Figure 7 shows the projections of this resolution volume for different

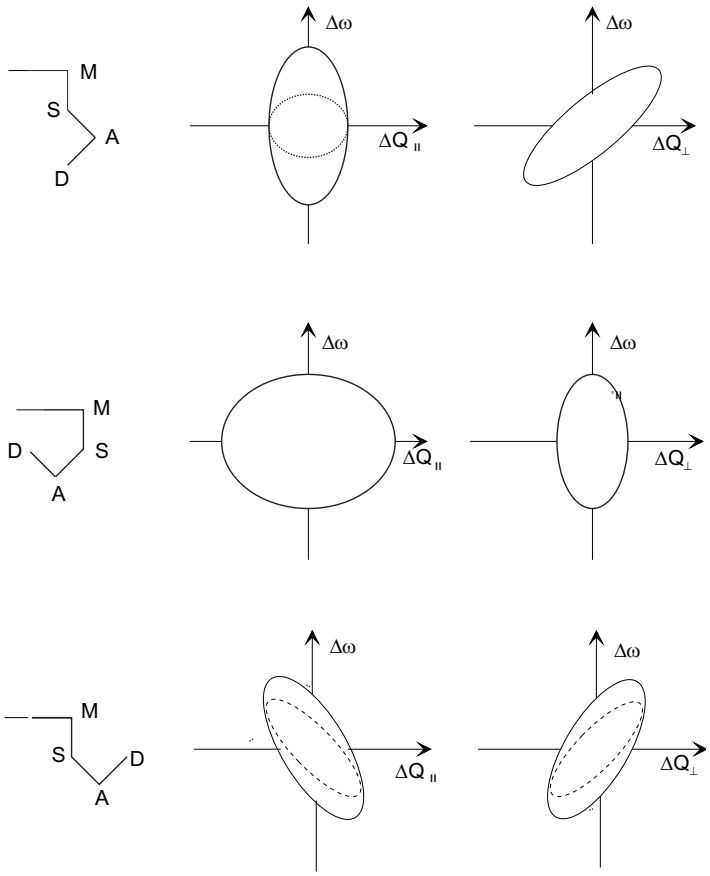

Figure 7. Different scattering geometries of a three-axis spectrometer with the corresponding projections of the resolution volume on the scattering plane and on its perpendicular plane. M is the monochromator, S the sample, A the analyser and D the detector.

spectrometer configurations. But for the case of a three-axis spectrometer in backscattering geometry (Alefeld *et al* 1968, Heidemann 1970), an inclination-free resolution volume $R(\boldsymbol{Q}, \omega)$ is achieved by using Bragg angles of 90° at the monochromator and analyser. This holds also for x-ray spectrometers working close to backscattering.

Figure 8 shows phonon dispersion curves in an arbitrary Brillouin zone and illustrates constant-$\boldsymbol{Q}$ scans for the standard neutron case and for x-rays with phonons to be observed at a certain phonon wavevector $\boldsymbol{q}$. Besides the different inclination, the size of the resolution volume varies for neutrons and is constant for x-rays. This is due to the strong variation of the wavevector $\boldsymbol{k}_f$ with energy transfer for neutrons. Therefore, the resolution volume has to be optimized experimentally for the corresponding energy and dispersion of the mode.

In an x-ray experiment the magnitude of the energy transfer has no influence on the resolution function.

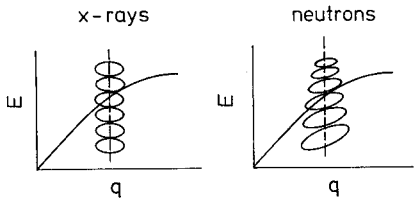

Figure 8. The behaviour of the resolution volume in constant-$\boldsymbol{Q}$ scans for the measurement of a phonon dispersion branch with neutrons and x-rays shown in an arbitrary Brillouin zone.

3.2. Phonons in single crystals

3.2.1. Phonons in beryllium. Apart from diamond (Burkel *et al* 1986, Dorner *et al* 1987), beryllium was the first crystal which was used to demonstrate the capabilities of inelastic x-ray scattering.

The longitudinal (L) modes of beryllium in the [00ξ] direction are particularly suited for investigations in Brillouin zones of (00l) type. The structure factor is either zero or $4f^2(Q)Q^2$, depending on l and on whether the mode is acoustic or optical. This is due to the fact that Bragg intensities at (00l) in an hcp structure with two atoms per primitive unit cell are extinguished for odd l and are proportional to $4f^2(Q)$ for even l. Therefore, the longitudinal acoustic (LA) modes can only be observed in zones with even l and the longitudinal optical (LO) modes in zones with odd l. In an extended zone scheme, the longitudinal modes present a continuous dispersion curve from one Γ point to the next Γ point.

Figure 9 shows energy scans for different scattering vectors $\boldsymbol{Q}$ with elastic and inelastic scattering intensities. The inelastic part clearly shows the longitudinal phonon excitation with its dispersion in $\boldsymbol{Q}$.

The complete dispersion curves of the longitudinal and transverse modes along the [00ξ] direction are shown in figure 10. The agreement of the x-ray data with the neutron data (dotted line) from Stedman *et al* (1976) shows that the two methods, x-ray and neutron scattering, lead to the same frequencies of the phonons. Therefore, the validity of the adiabatic approximation is a good assumption.

3.2.2. Phonons in α-SiO_2. For the demonstration of the strength and reliability of the new technique of inelastic x-ray scattering the phonon dynamics in single-crystalline α-quartz is well suited. It has hexagonal structure and its unit cell contains three SiO_2 units leading to

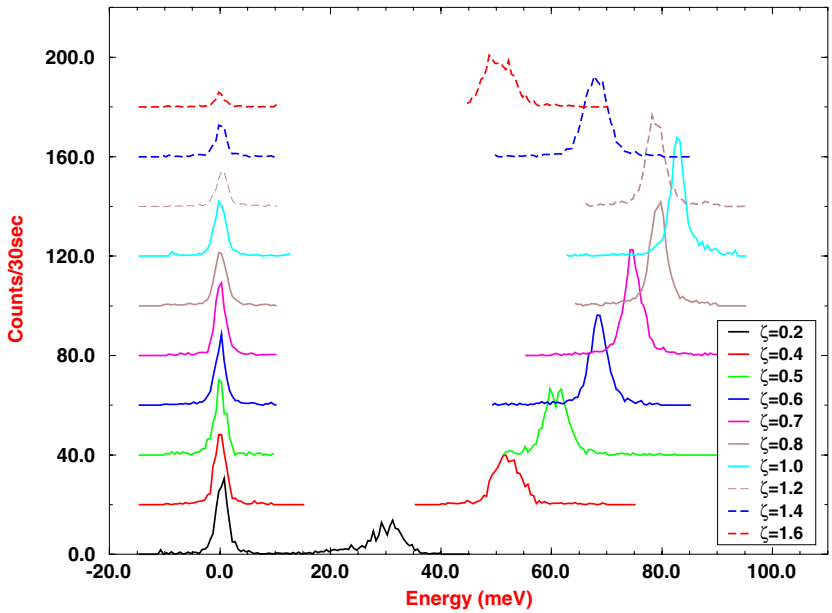

Figure 9. Energy scans at different values of Q in beryllium showing the inelastic scattering contributions from longitudinal phonons and elastic scattering.

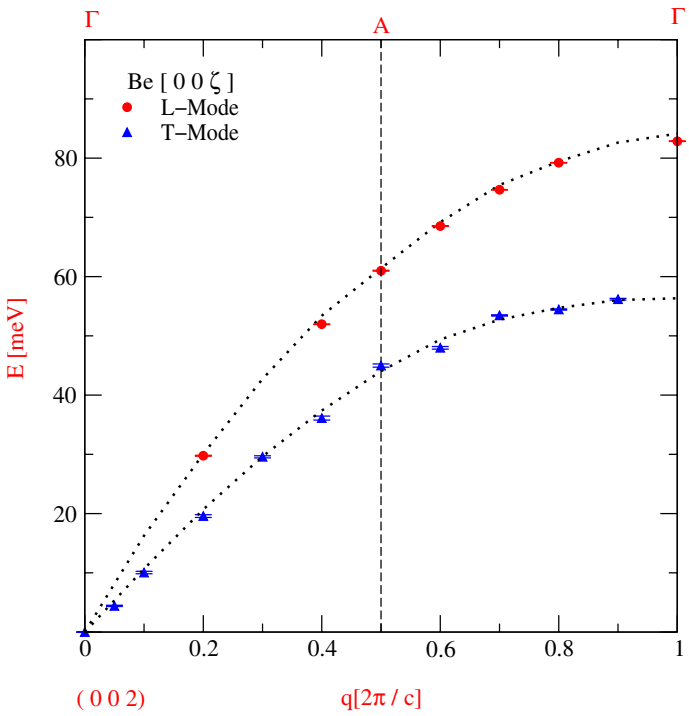

Figure 10. Phonon dispersion curves for the longitudinal and the transverse modes in beryllium along the [00ξ] direction as obtained with x-ray scattering by Sinn *et al* (2001) together with neutron data from the literature (Stedman *et al* 1976).

27 phonon branches along general crystal directions. However, along the Γ–K–M direction $[\zeta, 0, 0]$ selection rules reduce these to only 13 visible branches. The investigations were done along this direction (Halcoussis *et al* 1996, Halcoussis 1997, Burkel *et al* 1998, 1999).

Figure 11 gives the x-ray intensity scattered from α-SiO_2 at $\boldsymbol{Q} = (1.15\,0\,0)$ as a function of the energy transfer. It shows very strong signals from the longitudinal mode and from several higher-energy modes. The different modes were fitted with Lorentzian lines.

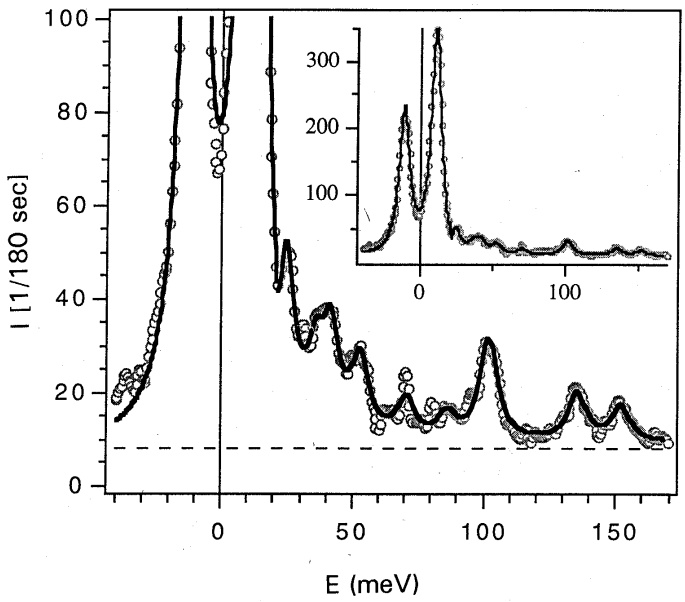

Figure 11. An energy scan at $\boldsymbol{Q} = (1.15\,0\,0)$ for α-SiO_2. The solid line is a fit and the inset shows the whole spectrum. The solid line is a fit and the dashed line represents the background. From Halcoussis (1997).

In figure 11, there are modes up to energies of 150 meV clearly visible above the background. This is a particular strength of the inelastic scattering technique using synchrotron radiation. It is possible to scan from zero energy transfer up to values well above 100 meV without changing the scattering geometry and even include energy-gain and energy-loss signals. Although the intensities of the modes decrease with higher energies, according to (8), they are visible with x-rays.

Figure 12 shows the energy values of the longitudinal modes obtained along the $[\zeta, 0, 0]$ direction of α-SiO_2 in very good agreement with the theoretical dispersion branches according to the shell model of Schober and Strauch (1993).

For the description of the lattice dynamics of a crystal, various theoretical approaches can be taken and the results compared with the experimental data. In general, the energies of the phonons are compared and optimized by variations of the model parameters.

However, inelastic scattering experiments with x-rays give access not only to the energies of the different modes but also to their intensities. This is simplified by the fact that the phonon signals have the same widths since the instrumental resolution function stays the same during the whole energy scan. Therefore, energy eigenvalues and eigenvectors of the modes are easily accessible. Figure 13 shows the dynamical structure factor ($G(\boldsymbol{Q}, \boldsymbol{q})$; see (7)) for the longitudinal acoustic mode along $[\zeta, 0, 0]$ for x-rays and neutrons calculated by Halcoussis (1997). The eigenvectors were taken from the shell model by Schober and Strauch (1993)

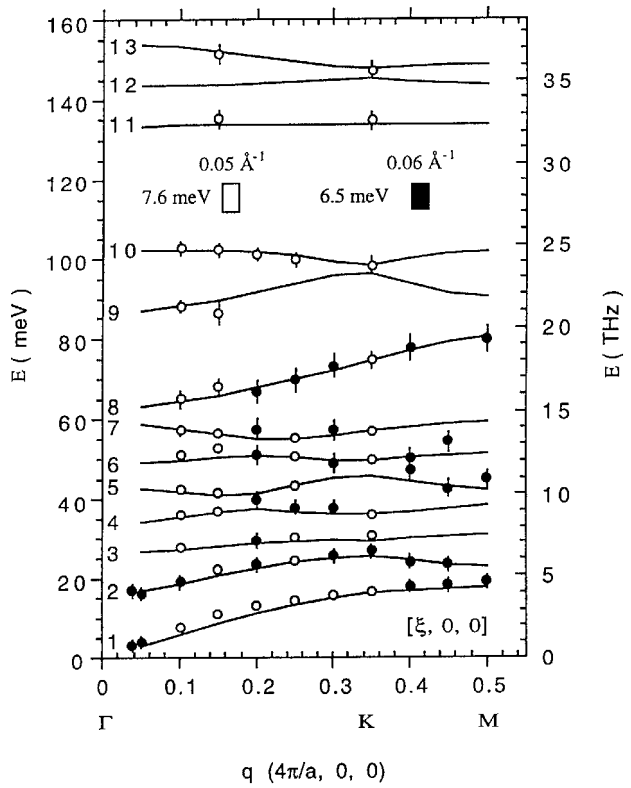

Figure 12. Phonon dispersion curves of α-SiO_2 along ΓKM together with results according to a shell model (Schober and Strauch 1993). From Halcoussis (1997).

which was optimized by using only energy values obtained in the neutron experiments.

The high sensitivity of inelastic x-ray scattering opens up the possibility of studying the behaviour of the eigenvectors in more detail. The eigenvectors $e_d(\boldsymbol{q}, j)$ are complex, describing the modulus and the phase of the phonon. This means that for a certain polarization, the imaginary part can lead to a phase shift of the scattering atoms. Thus, the constructive interference in the long-wavelength limit ($q \rightarrow 0$), where all atoms are in phase, can change to destructive interference with increasing q. For instance, the atoms can be out of phase already in the acoustic mode and vibrate in antiphase, similarly to in an optical mode. Since the momentum transfer q is changing its sign at a lattice point, the effect may be different for momentum transfers Q smaller or larger than a certain lattice vector. Such effects are visible in figure 13 as strong asymmetries in the intensities around the lattice vectors (1, 0, 0), (2, 0, 0) and (3, 0, 0) in a very pronounced way. Halcoussis (1997) confirmed this behaviour experimentally around (1, 0, 0).

In addition to these experiments some neutron inelastic measurements were performed using the triple-axis spectrometer IN3 at the high-flux reactor at the Institut Laue–Langevin (ILL) at Grenoble. Therefore, the experiments on α-SiO_2 allow a direct comparison between inelastic scattering with x-rays and neutrons (table 1).

It is remarkable that despite the difference of six orders of magnitude in the scattering volume, phonon spectra with similar statistics can be obtained in equal times. The reported results on α-SiO_2 obtained with inelastic x-ray scattering were gained on a sample of only

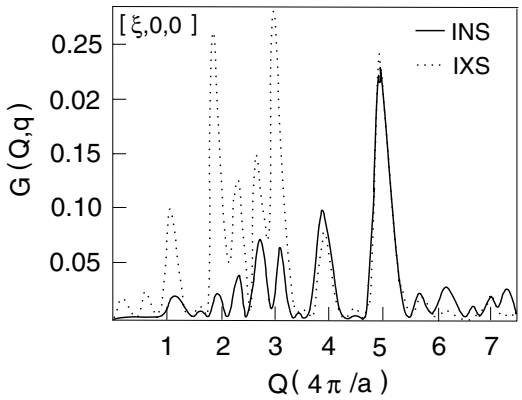

Figure 13. The structure factor ($G(\boldsymbol{Q}, \boldsymbol{q})$ of α-SiO_2 for the longitudinal acoustic mode along $[\zeta, 0, 0]$ for x-rays (broken line) and neutrons (full line) calculated by Halcoussis (1997).

Table 1. Comparison of x-ray and neutron scattering. The data are taken from Halcoussis (1997).

	Neutrons	Photons
Flux at sample position	10^7 cm^{-2} s^{-1}	10^{10} mm^{-2} s^{-1}
Scattering volume	6×10^4 mm^3	5×10^{-2} mm^3
Count rate for a typical LA phonon at maximum	215 min^{-1}	117 min^{-1}
time for a scan range of 10 meV transfer	60 min	65 min

5×10^{-2} mm^3 scattering volume.

Due to this sensitivity of the x-ray method to the intensities of the phonons, considerable knowledge can be gained about the eigenvectors and, thus, improvements in the modelling techniques of lattice dynamics are expected.

3.2.3. Phonons in He. Solid and liquid helium are ideal systems for the study of the influence of quantum effects in condensed matter. In particular, the dynamics of these quantum systems is a subject of continuous interest. In the case of solid helium, the mass-dependent zero-point vibrations are very important for the dynamics of both isotopes. Therefore, the comparison of the phonon spectra and the dispersion curves for the two isotopes, ^{3}He and ^{4}He, is essential to test the theoretical description of these highly anharmonic systems. However, inelastic neutron scattering—the common method for studying the dynamics in solids—could only deliver results on solid ^{4}He. Due to the very high absorption cross section for unpolarized thermal neutrons, solid ^{3}He was not yet accessible. This restriction does not apply for inelastic x-ray scattering.

The experiments (Burkel *et al* 1995, Schell *et al* 1996, Seyfert *et al* 1996, Seyfert 1998, Seyfert *et al* 1999, Burkel *et al* 1999) were performed on single crystals in the hcp phase for both isotopes at a density of 13.25 cm^3 mol^{-1}. Due to the high zero-point energy, helium can only be solidified under pressure even at the lowest temperatures. Therefore, the crystals were grown *in situ* in a polycrystalline Be cell of 1.2 mm inner diameter (Venkataraman and Simmons 1996) within a closed-cycle refrigerator. The Be cell was pressurized through a steel capillary from the external pressure-generating system. At constant pressures of 70 and 90 MPa, the cell was cooled down below the freezing temperature of helium. The crystals

were characterized and oriented using their Bragg reflections.

Longitudinal phonons were detected in crystals of both isotopes at momentum transfers from 6 to 23.5 nm^{-1}. Some spectra along the c-axis are shown in figure 14 (top) for hcp ^{3}He and for hcp ^{4}He (bottom). Beyond the elastic scattering intensity of the Be cell at energy transfer $\omega = 0$ the contributions of the helium phonons are clearly visible and their dispersion obvious. The lineshapes can be very well described within the model of a damped harmonic oscillator (Fak and Dorner 1992).

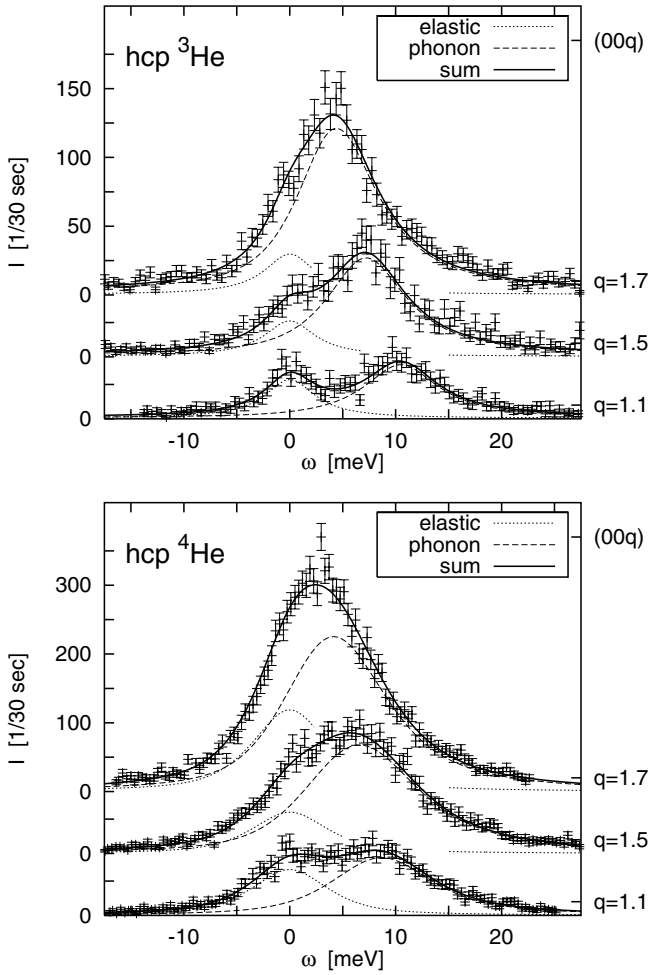

Figure 14. Inelastic x-ray spectra of hcp ^{3}He and ^{4}He for different momentum transfers along the [001] direction. The data were taken with energy resolutions of 5.9 meV and 8.6 meV, respectively. Solid lines are fits to the data (Seyfert 1998).

Figure 15 shows the longitudinal dispersion relations for phonons along the [001] direction in hcp crystals of both isotopes. The dispersion curves are similar but the phonon frequencies in ^{3}He are about 11(5)% higher than in ^{4}He. This value is smaller than the ratio expected in a classical harmonic crystal, i.e., from the square root of the inverse masses, $\sqrt{4/3} = 1.154$. Thermodynamic measurements (Ahlers 1970) and Raman spectroscopy (Slusher and Surko 1976) delivered even higher values of 1.18 and 1.17, respectively. These differences could be

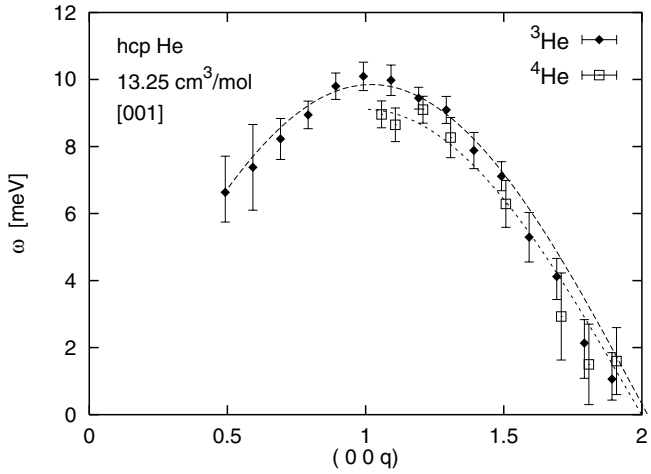

Figure 15. Comparison of the dispersion curves of the longitudinal modes in hcp ^{3}He and hcp ^{4}He. From Seyfert (1998).

an indication of a mode-dependent frequency ratio.

In addition to the phonon frequencies it was also possible to determine the linewidths. Figure 16 gives the deconvoluted intrinsic widths of the excitations along the [001] direction for both helium isotopes as functions of the momentum transfer. The absolute values of the widths and their variations with the momentum transfer are similar within the experimental error bars. There is no significant broadening at low momentum transfers. At moderate momentum transfers, however, there is considerable broadening observed. This behaviour is attributed to unresolved multi-phonon contributions. These contributions can also be responsible for the

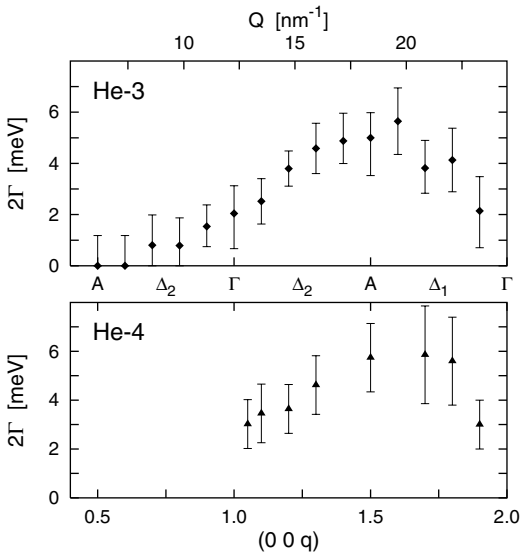

Figure 16. Linewidths of the longitudinal phonons in hcp ^{3}He and hcp ^{4}He. From Seyfert (1998).

observed asymmetry of the phonon dispersion around the lattice point A in figure 15.

The comparison of the results with theoretical approaches reveals that hcp helium is not yet described in a satisfactory way. The observed phonon frequencies in hcp ^{3}He are about 20–30% lower than predicted in the only available calculation (Morley and Kliewer 1969). The frequencies of hcp ^{4}He are reproduced to about 10–15% of a calculation (Gillis *et al* 1968). Besides, there is a noticeable discrepancy between the experiment and these models as regards the dependence of the phonon frequencies. Moreover, no theoretical study of phonon lineshapes in hcp helium has been published yet.

3.2.4. Phonons in large-band-gap materials. Large band-gap III–V nitride semiconductors are materials suited for applications in high-temperature electronics and for optical applications at short wavelengths, since they show high-temperature stability.

Experiments on a AlN single crystal, only available in the wurtzite phase, with the approximate dimensions $(0.5 \times 0.5 \times 0.5)$ mm^3 by Schwoerer-Böhning *et al* (1999) led to the dispersion curves of longitudinal and transverse phonons shown in figure 17. First-principles calculations performed by the authors are given as solid lines in the figure. The calculated density of states is shown as well. There is an excellent agreement between the data and the calculations. For further details see Schwoerer-Böhning *et al* (1999).

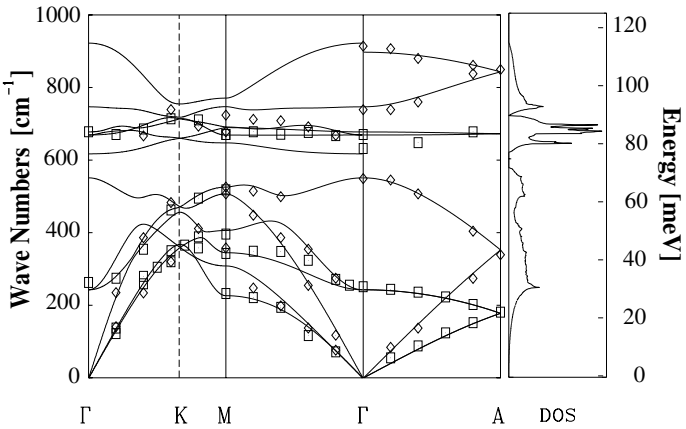

Figure 17. Longitudinal acoustic and optical phonon dispersions of wurtzite AlN together with the results from *ab initio* calculations from Schwoerer-Böhning *et al* (1999).

3.3. Phonons in polycrystals

Polycrystals contain a variety of randomly oriented single crystallites. There is no distinct orientational direction as in single crystals and, therefore, the direction of the momentum transfer $\hbar\boldsymbol{Q}$ relative to the crystal orientation is not defined. Because of the averaging over the orientation only the absolute value, $|\boldsymbol{Q}| = Q$, is defined. This means that the scattering process takes place on a spherical shell in the reciprocal space and not on a point, as in the case of single crystals. In an elastic scattering process the shells are observed as Debye–Scherrer rings. This is illustrated in figure 18, contrasting with figure 4. There can be fine structure of the rings, depending on the grain size of the crystallites and on the resolution volume.

The attempt to measure phonons (Burkel *et al* 1990, Burkel 1991) with a certain momentum transfer can lead to contributions from a variety of phonon modes depending

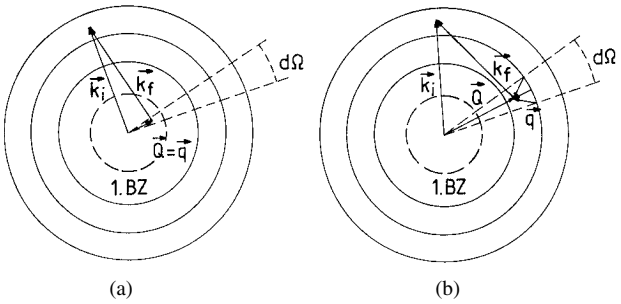

Figure 18. The scattering geometry in a polycrystal for the observation of phonons for momentum transfer $\boldsymbol{Q}$ in the reciprocal space within the first Brillouin zone (a) and beyond (b).

on the value of Q and on the solid angle $\mathrm{d}\Omega$ (figure 6). In order to obtain a dispersion relation of a material, one needs a distinct correlation of the wavevector $\boldsymbol{q}$ with its frequency ω. In a polycrystalline material this is only possible in the first Brillouin zone with the reciprocal-lattice vector $\boldsymbol{\tau}$ equal to 0, which leads to the fact that the momentum transfer $\hbar Q$ equals $\hbar q$. This shows that only longitudinal (compression) phonon modes are measured within the first Brillouin zone (figure 18(a)). Any momentum transfer beyond the first Brillouin zone will excite several longitudinal and transverse phonon modes simultaneously and the result will be a scattering spectrum which gives information on the density of states of these vibrational modes (figure 18(b)).

3.3.1. Polycrystalline H_2O ice, I_h. Polycrystalline H_2O ice I_h was investigated using inelastic scattering of x-rays by Ruocco *et al* (1996) and Sette *et al* (1996).

Data taken at -10°C with an energy resolution of 3.2 meV are shown in figure 19 together with fit curves at different momentum transfers.

The well defined peaks indicating the presence of only a few grains in the sample are interpreted as gain and loss signals of longitudinal and transverse modes. The derived dispersion curves are shown in the inset of figure 19.

The longitudinal mode is visible at all momentum transfers, whereas the transverse mode is visible only beyond a momentum transfer of 7 nm^{-1}. This coincides with about the smallest size of the reduced Brillouin zone in ice. However, one has to be careful that the energy resolution might not be sufficient to resolve details below this value.

3.3.2. Acoustic phonon dispersion in CdTe at 7.5 GPa. Hydrostatic pressure is an increasingly important parameter in the study of matter since it allows one to correlate macroscopic thermodynamic parameters with interparticle properties and to derive the equation of state. Aside from structural questions, there is also the aim of gaining knowledge of the behaviour of interatomic force constants. Such information is obtained by the study of the dynamics under pressure. However, inelastic neutron scattering experiments require large sample volumes which limits them to pressures of about 10 GPa for single crystals and about 30 GPa for powder samples (Besson *et al* 1992). In contrast to this, the small size of an x-ray beam allows working with small samples of μm dimensions enclosed in diamond anvil cells.

Since the development of the inelastic x-ray method, attempts have been made to study the dynamics under pressure. Because of the large focus size at the HASYLAB instrument, a modified Paris–Edinburgh pressure cell (Besson *et al* 1992), normally used for large sample volumes in neutron scattering experiments, was used. The longitudinal phonons in single-

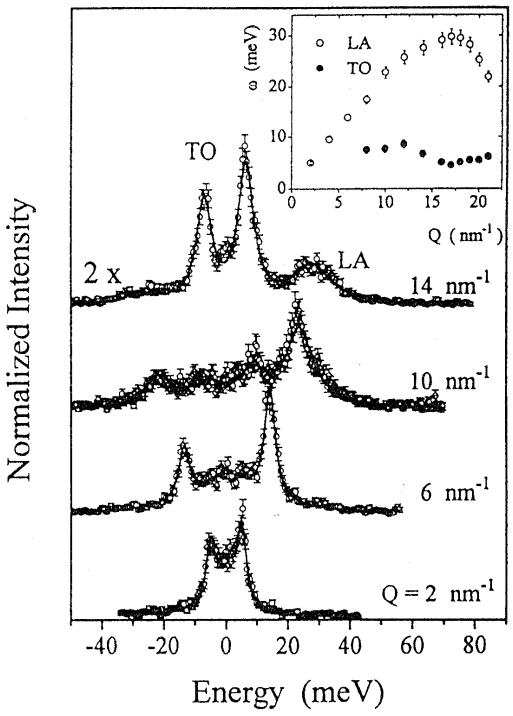

Figure 19. Inelastic x-ray scattering data of polycrystalline H_2O ice I_h at -10 °C at different momentum transfers together with fit curves. The inset shows the derived mode dispersion curves, taken from Sette *et al* (1996).

crystalline Si embedded in LiF were resolved at a pressure of 4 GPa by Schwoerer-Böhning (1995) and Burkel *et al* (1995).

Recently, the diamond anvil cell technology was applied by Krisch *et al* (1997) in the study of the dynamics in polycrystalline CdTe in its sodium chloride phase (Nelmes *et al* 1995) at a pressure of 7.5 GPa at room temperature. The size of the photon beam was $100 \times 100\ \mu m^2$ and the energy width was 5 meV. The longitudinal acoustic branch could be observed up to 10 nm^{-1}, just beyond the first Brillouin zone. The dispersion curve obtained is shown in figure 20 together with results from inelastic neutron scattering for the zinc-blende phase of CdTe at ambient pressure for the crystallographic [111], [100] and [110] directions. There is a strong increase of the excitation energies in the high-pressure phase compared to the one at ambient pressure. The velocity of sound determined by a fit to the data using a sine function increased from 3200 m s^{-1} to 5100 m s^{-1}. Furthermore, the Grüneisen parameter could be derived.

These results clearly demonstrate the capabilities of inelastic x-ray scattering experiments in the field of high-pressure research.

4. Concluding remarks

These few examples clearly demonstrate the capability of high-energy-resolution spectroscopy with synchrotron radiation of determining the dispersion of vibrational modes in crystalline solids. Certainly, this technique is well suited for studying such excitations also in materials lacking any translational lattice symmetry like amorphous, glassy or liquid materials, as demonstrated in other contributions in this Special Issue.

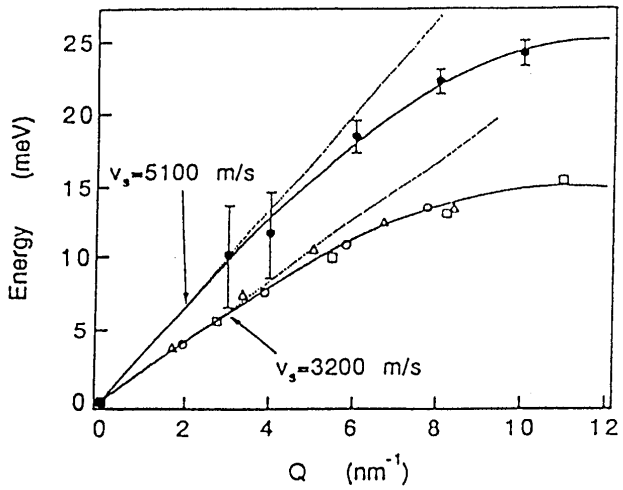

Figure 20. The phonon dispersion curves of CdTe at 7.5 GPa (●: x-ray data, Krisch *et al* 1997) and at ambient pressure (△: along [111]; ○: along [100]; and □: along [110], Rowe *et al* 1974). The solid lines represent a fit and the dotted line indicates the derived velocities of sound. From Krisch *et al* (1997).

Acknowledgments

Part of the work described was supported by the BMBF under the contracts 05 650 HRA 1 and 05 643 HRA 5 and by a DAAD-NSF grant.

References

Ahlers G 1970 *Phys. Rev.* A **2** 1505
Alefeld B, Birr M and Heidemann A 1968 *Neutron Inelastic Scattering* (Vienna: IAEA) p 381
Bacon G E 1962 *Neutron Diffraction* 2nd edn (Oxford: Clarendon)
Besson J M, Nelmes R J, Hamel G, Loveday J S, Weill G and Hull S 1992 *Physica* B **180+181** 907
Born M 1942 *Rep. Prog. Phys.* **9** 356
Brockhouse B N 1961 *Inelastic Scattering of Neutrons in Solids and Liquids* (Vienna: IAEA) pp 531–48
Brockhouse B N, Arase T, Caglioti G, Rao K R and Woods A D B 1962 *Phys. Rev.* **128** 1099
Brüsch P 1982 *Phonons I (Springer Series in Solid State Sciences)* (Berlin: Springer)
Brüsch P 1986 *Phonons II (Springer Series in Solid State Sciences)* (Berlin: Springer)
Brüsch P 1987 *Phonons III (Springer Series in Solid State Sciences)* (Berlin: Springer)
Burkel E 1989 *X-Ray Instrumentation in Medicine and Biology, Plasma Physics, Astrophysics and Synchrotron Radiation (Proc. SPIE vol 1140)* ed R Benattar (Bellingham, WA: SPIE) p 426
Burkel E 1991 *Inelastic Scattering of X-Rays with Very High Energy Resolution (Springer Tracts in Modern Physics vol 125)* (Berlin: Springer)
Burkel E 2000 *Rep. Prog. Phys.* **63** 171
Burkel E, Dorner B, Illini Th and Peisl J 1987a *HASYLAB Annual Report* p 337
Burkel E, Dorner B, Illini Th and Peisl J 1989 *Rev. Sci. Instrum.* **60** 1671
Burkel E, Dorner B, Illini Th and Peisl J 1991 *J. Appl. Crystallogr.* **24** 1042
Burkel E, Gaus S, Illini Th and Peisl J 1990 *PHONONS 89 Conf. Proc.* vol 2 (Singapore: World-Scientific) p 1436
Burkel E, Halcoussis H and Sinn H 1998 *Strongly Coupled Coulomb Systems* ed G J Kalman, J M Rommel and K B Blagoev (New York: Plenum) p 123
Burkel E, Illini Th, Peisl J and Dorner B 1986 *HASYLAB Annual Report* p 383
Burkel E, Peisl J and Dorner B 1987b *Europhys. Lett.* **3** 957
Burkel E, Schwoerer-Böhning M, Seyfert C and Simmons R O 1995 *Physica* B **219+220** 98
Burkel E, Seyfert C, Halcoussis C, Sinn H and Simmons R O 1999 *Physica* B **263+264** 412

Cochran W and Cowley R A 1967 Phonons in perfect crystals *Handbuch der Physik* vol XXV/2a, ed L Genzel (Berlin: Springer)
Cooper M J and Nathans R 1967 *Acta Crystallogr.* **23** 357
Dorner B 1972 *Acta Crystallogr.* A **28** 319
Dorner B, Burkel E, Illini Th and Peisl J 1987 *Z. Phys.* B **69** 179
Fak B and Dorner B 1992 *Institut Laue–Langevin, Grenoble, Technical Report* No 92FA0085
Gillis N-S, Koehler T-R and Werthamer N-R 1968 *Phys. Rev.* **175** 1110
Halcoussis Ch 1997 *PhD Thesis* University of Rostock
Halcoussis Ch, Sette F, Burkel E, Krisch M, Masciovecchio C, Sinn H and Verbeni R 1996 *Conf. Proc. 5ème Journées de la Matière Condensée (Orléans, France)*
Heidemann A 1970 *Z. Phys.* **238** 208
Holt M, Wu Z, Hong H, Zschack P, Jemian P. Tischler J, Chen H and Chiang T C 1999 *Phys. Rev. Lett.* **83** 3317
Horton G K and Maradudin A A 1974 *Dynamical Properties of Solids* vol 1 (Amsterdam: North-Holland)
Joynson R E 1954 *Phys. Rev.* **94** 851
Krisch M, Mermet A, San Miguel A, Sette F, Masciovecchio C, Ruocco G and Verbeni R 1997 *Phys. Rev.* B **56** 8691
Lovesey S W and Springer T (ed) 1977 *Dynamics of Solids and Liquids by Neutron Scattering (Springer Topics in Current Physics vol 3)* (Berlin: Springer)
Morley G-L and Kliewer K-L 1969 *Phys. Rev.* **180** 245
Nelmes R J, McMahon M I, Wright N G and Allan D R 1995 *Phys. Rev.* B **51** 15 723
Peierls R E 1955 *Quantum Theory of Solids* (Oxford: Clarendon)
Rowe J M, Nicklow R M, Price D L and Zanio K 1974 *Phys. Rev.* B **10** 671
Ruocco G, Sette F, Mazzacurati V, Signorelli G and Verbeni R 1996 *Nature* **379** 521
Schell N, Simmons R-O and Burkel E 1996 *J. Synchrotron Radiat.* **3** 316
Schober H and Strauch D 1993 *J. Phys.: Condens. Matter* **5** 6165
Schwoerer-Böhning M 1995 *Thesis* Universität Erlangen–Nürnberg
Schwoerer-Böhning M, Macrander A T, Pabst M and Pavone P 1999 *Phys. Status Solidi* b **215** 177
Sette F, Ruocco G, Krisch M, Masciovecchio C, Verbeni R and Bergmann U 1996 *Phys. Rev. Lett.* **74** 83
Seyfert C 1998 *Thesis* University of Rostock
Seyfert C, Arms D A, Sinn H, Simmons R O and Burkel E 1996 *Czech. J. Phys. Suppl.* S1 **46** 471
Seyfert C, Simmons R O, Sinn H, Arms D A and Burkel E 1999 *J. Phys.: Condens. Matter* **11** 3501
Sinn H, Alp E E, Alatas A, Barraza J, Bortel G, Burkel E, Shu D, Sturhahn W, Sutter J P and Toellner T S 2001 *Nucl. Instrum. Methods* A at press
Slusher R-E and Surko C-M 1976 *Phys. Rev.* B **13** 1086
Stedman R, Amilius Z, Pauli R and Sundin O 1976 *J. Phys. F: Met. Phys.* **6** 157
Van Hove L 1954 *Phys. Rev.* **95** 249
Venkataraman C T and Simmons R O 1996 *Rev. Sci. Instrum.* **67** 3365
Walker C B 1956 *Phys. Rev.* **103** 547